

# An Analysis of Complex-Valued CNNs for RF Data-Driven Wireless Device Classification

Jun Chen<sup>†</sup>, Weng-Keen Wong<sup>†</sup>, Bechir Hamdaoui<sup>†</sup>, Abdurrahman Elmaghbab<sup>†</sup>, Kathiravetpillai Sivanesan<sup>‡</sup>, Richard Dorrance<sup>‡</sup>, Lily L. Yang<sup>‡</sup>

<sup>†</sup> Oregon State University, Corvallis, OR, USA; Email: {chenju3,wongwe,hamdaoui,elmaghba}@oregonstate.edu

<sup>‡</sup> Intel Corporation, Hillsboro, OR, USA; Email: {kathiravetpillai.sivanesan,richard.dorrance,lily.l.yang}@intel.com

**Abstract**—Recent deep neural network-based device classification studies show that complex-valued neural networks (CVNNs) yield higher classification accuracy than real-valued neural networks (RVNNs). Although this improvement is (intuitively) attributed to the complex nature of the input RF data (i.e., IQ symbols), no prior work has taken a closer look into analyzing such a trend in the context of wireless device identification. Our study provides a deeper understanding of this trend using real LoRa and WiFi RF datasets. We perform a deep dive into understanding the impact of (i) the input representation/type and (ii) the architectural layer of the neural network. For the input representation, we considered the IQ as well as the polar coordinates both partially and fully. For the architectural layer, we considered a series of ablation experiments that eliminate parts of the CVNN components. Our results show that CVNNs consistently outperform RVNNs counterpart in the various scenarios mentioned above, indicating that CVNNs are able to make better use of the joint information provided via the in-phase (I) and quadrature (Q) components of the signal.

<sup>1 2</sup>

## I. INTRODUCTION

Radio frequency (RF) fingerprinting has emerged as a key enabler for providing automated device identification proven useful in a wide range of new wireless applications [1], [2], [3]. In essence, RF fingerprinting extracts features from transmitted RF signals to distinguish between different devices [4], [5]. Traditionally, RF fingerprinting relies on carefully hand-crafted features that require domain knowledge of the underlying communication (e.g., modulation) protocols. Recently, a growing number of deep learning-based algorithms have been proposed for RF wireless signal classification (see Section II). Unlike the traditional approach, recent deep learning approaches learn a representation directly from the raw IQ samples of wireless signals and thus do not rely on any domain knowledge to construct features. These deep learning methods show strong benefits in applying neural networks to wireless signal classification tasks.

While much of the existing literature in this area has focused on using real-valued neural networks (RVNNs) [2], [6], some researchers have shown that complex-valued neural

networks (CVNNs) [7], [8], which account for the complex-valued aspects of the data, can be more effective. Although these approaches show that CVNNs can outperform RVNNs, a deeper analysis providing insights into why CVNNs are more effective than RVNNs is still lacking.

In this work, we study RVNNs and CVNNs vis-a-vis of their ability to identify and classify wireless devices using RF signals collected from real-world datasets capturing two widely used protocols, LoRa and WiFi. Specifically, we compare the performances of CVNNs and RVNNs and perform a deeper analysis of the benefits of CVNNs through a series of experiments, including ablation experiments that remove parts of the CVNN architecture to understand which parts of the network have the most impact on its predictive performance. Our experimental results show that:

- CVNNs consistently outperform their "equivalent" (in terms of the number of neural network parameters) RVNNs on RF/device classification tasks under various experimental settings.
- CVNNs are able to exploit the joint In-phase (I) and quadrature (Q) feature information of the RF signals more effectively than RVNNs.
- In general, ablated CVNNs yield lower accuracy, which indicates that removing cross-terms causes information loss and makes CVNNs behave like RVNNs.
- Ablated CVNNs exhibit decreasing trends in performance with higher layers being ablated, indicating that similar to RVNNs, deeper layers of CVNNs contain higher-level features that result in higher accuracy.
- In some cases, removing part of the layer improves accuracy. This break in the decreasing trend makes us speculate that the additional cross-terms of CVNNs can not only enrich information but also increases the redundancy of information and harm the performance.

The remainder of this paper is organized as follows. Section II describes the related works applying deep learning approaches on RF signal/device classification. Section III describes the datasets used in our evaluation. Section IV presents the detailed neural networks configuration and ablation strategies used in this work. Experimental results are discussed in Section V and Section VI concludes the paper.

<sup>1</sup>This work is supported in part by NSF/Intel Award No. 2003273.

<sup>2</sup>©2022 IEEE. Personal use of this material is permitted. Permission from IEEE must be obtained for all other uses, in any current or future media, including reprinting/republishing this material for advertising or promotional purposes, creating new collective works, for resale or redistribution to servers or lists, or reuse of any copyrighted component of this work in other works.

## II. RELATED WORK

Early works on RF fingerprinting focused on automatic modulation classification and on using model based approaches to hand-craft and design features [6], [9], [10]. More recent RF fingerprinting works have shifted towards using deep learning to extract features from RF signals automatically [2], [4], [11], [12], [13], [14]. For instance, Soltani et al. [13] proposed a data augmentation method for raw IQ data samples that works without needing prior knowledge about the waveform and the receiver-transmitter coordination. The approach proposed in [4], [5] leverages out-of-band spectrum emissions that are caused by hardware impairments to enhance fingerprinting accuracy. Al-Shawabka et al. [15] investigate the impact of the wireless channel on fingerprinting accuracy.

Some approaches used CVNNs instead of RVNNs to enable fingerprinting [7], [16]. For example, Gopalakrishnan et al. [7] employed CVNN for RF fingerprinting and showed the benefits of the preamble and noise augmentation on the accuracy. The CVNN architecture used in [7] is a hybrid neural network that inserts real-valued layers after complex convolutional layers. Agadakos et al. [16] developed two novel deep CVNNs (DCN) that are agnostic of the underlying protocols. They found that these CVNNs outperform their real-valued counterparts, even with fewer parameters. However, the authors did not provide the details of their neural network models, nor did they provide a deeper analysis of why the CVNN is better than RVNN. Unlike past work, our paper, for the first time, will focus on a detailed analysis of why the CVNNs are a better choice for RF fingerprinting.

## III. RF DATASETS

We next provide brief descriptions of the LoRa and WiFi RF datasets used for our evaluation, which are collected respectively at Oregon State University [17] and at Northeastern University [15], with further details found in the corresponding references.

### A. LoRa Dataset Scenarios

We consider two LoRa dataset scenarios, LoRa/In and LoRa/Out, collected using a testbed comprised of 25 Pycom transmitters and USRP B210 receivers. For a detailed description of the full datasets, refer to [17].

- LoRa/In: This is an indoor environment scenario, where RF samples are captured from the 25 Pycom devices, each transmitting the same message from the same location, 5m away from the receiver. For more details, refer to Setup 1 in [17].
- LoRa/Out: To allow for performance evaluation while considering the impact of outdoor wireless channel impairments, we also considered an outdoor environment scenario. In this scenario too, all devices transmit the same message from the same location, 5m away from the receiver. For more details, refer to Setup 2 in [17].

### B. WiFi Dataset Scenarios

The previous two dataset scenarios focus on LoRa device fingerprinting. For completeness, we also consider the following

two dataset scenarios: Wired and WiFi [15].

- **Wired:** This dataset scenario (corresponding to Setup C in [15]) is collected by Northeastern University (NE) team using a testbed of 20 SDR (software define radios), composed of 13 N210 and 7 X310 USRPs. The data acquisition is done using a USRP N210 receiver with a sampling rate of 20MS/s. All transmitters were connected to the receiver using the same coaxial RF SMA cable and a 5db attenuator one at a time. By this setup all transmitters are not affected by multi-path and experience exactly the same channel conditions.
- **WiFi:** This dataset scenario (corresponding to Setup D in [15]), also provided by the same NE team, is collected using a testbed is constituted of 10 SDRs (4 N210 and 6 X310 USRPs). The devices are located in an anechoic chamber and are connected to the same transmitting antenna. The data acquisition is done using a USRP N210 receiver with a sampling rate of 20MS/s. Each device transmits the same IEEE 802.11 a/g packets for 30s, one at a time.

## IV. METHODOLOGY

We now describe our experimental methodology, which includes details on the datasets used, the neural network architectures and the experiments conducted.

### A. Dataset Construction for Experimental Evaluation

Typically, an evaluation methodology like averaging over multiple random train/test splits or cross-validation is used. However, RF data experiences changes in the data distribution over the duration of the transmission. This non-stationary behavior violates the assumptions of standard machine learning evaluation methodologies. Data from different transmissions from the same device can also exhibit quite a large variance. As a result, we need to create a specialized methodology suitable for our RF data-based experiments.

To mitigate the non-stationary behavior, we ensure that the training data is close in time to the test data. In addition, for each device, we restrict the training and test data to be from the same transmission. Consequently, we create  $S$  datasets which we refer to as *splits* and evaluate the average accuracy of these  $S$  splits. Suppose there are  $K$  devices (the number of classes) and we only use  $M$  transmissions per device in our experiments. To form splits, we create  $P$  train/test partitions in each transmission and these partitions are created from evenly-spaced time intervals over the transmission data. A split consists of the corresponding partitions of corresponding transmissions over all devices, where *corresponding* means the same index, as shown in Figure 1. To be specific, the *split* with index of  $P \times (m-1) + p$  is the union of the partition  $p$  in transmission  $m$  of all  $K$  devices, where  $m \in [1, \dots, M]$  and  $p \in [1, \dots, P]$ . Since we can form  $P$  splits per transmission over all devices, the total number of splits is  $S = P \times M$ .

We create the splits using the middle third of the data to avoid dealing with specialized data in the first or last third of the transmission. For one split, there are  $K$  partitions (1 partition from each of the  $K$  devices). Each partition contains

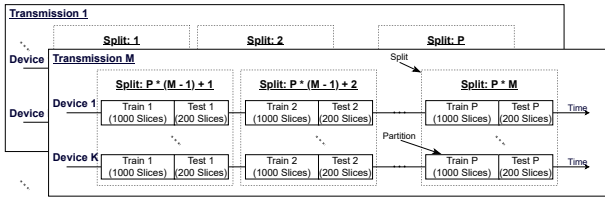


Fig. 1: Constructing splits from the data

1200 consecutive IQ samples at the beginning. We create 1200 overlapping sliding windows based on these consecutive IQ samples of partition, where we refer to the data within a window as a *slice*. Thus, using the first IQ sample of the partition as the starting point, we take a window of 100 samples as the first slice for a given device. Then, we advance the sliding window on the transmission in which the partition is by a stride of size 1 and take the next 100 samples as the second slice. This process continues until the last sample of the partition (as the starting point of the last slice). We repeat this process for each device. Each split is formed by taking the union of the generated slices from partition  $p$  from transmission  $m$  over all devices. The total number of slices from a split is  $1200 \times K$  and each slice has a dimension of  $2 \times 100$  because the IQ sample has the two parts of I and Q.

The ratio of training to test instances is 5 : 1 and we ensure that the training data has an equal number of slices from each device. The final results of our experiments evaluate and show the accuracy averaged over all  $S$  splits in each datasets scenario. For OSU-LoRa dataset scenarios  $K = 25, M = 1, P = 50, S = 50$  and for NE-Wired/WiFi dataset scenarios  $K = 20, M = 3, P = 50, S = 150$ .

### B. Complex-Valued Neural Networks: CVNNs

Early work on CVNNs used pure complex number operations and focused on the topics of complex activation functions [18], [19] and complex backpropagation [20], [21]; this work was primarily intended for shallow neural networks. Modern software packages for deep networks are largely built around automatic differentiation for real values. Software to extend automatic differentiation to complex values is not currently mature and often suffers from numerical instability. As a result, modern software packages attempt to reuse real-valued functionality to approximate complex-valued building blocks such as complex-valued convolutional layer, complex-valued ReLUs, and complex-valued batch normalization layer [22].

The most important component of a CVNN is the complex-valued convolutional layer which reflects the essential difference between the CVNNs and RVNNs. Each complex-valued convolutional block within the layer contains a complex filter matrix  $W = A + iB$  and an input vector  $h = x + iy$ ; here,  $A$  and  $B$  are real matrices while  $x$  and  $y$  are real vectors. The complex convolution can be expanded according the distributive property of convolution operator:

$$\mathbf{W} * \mathbf{h} = (\mathbf{A} * \mathbf{x} - \mathbf{B} * \mathbf{y}) + i(\mathbf{B} * \mathbf{x} + \mathbf{A} * \mathbf{y}) \quad (1)$$

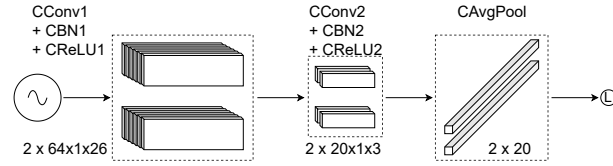
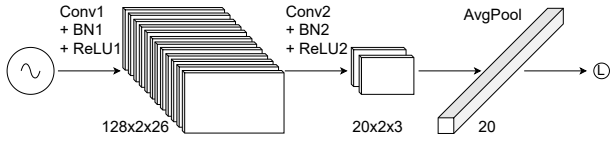


Fig. 2: Architecture of RVNN (top) and CVNN (bottom).

RVNN (Real-Valued CNN)			CVNN (Complex-Valued CNN)		
Layer Type	Output Size	Filter/Stride Size	Layer Type	Output Size	Filter/Stride Size
Input	$1 \times 2 \times 100$		Input	$2 \times 1 \times 1 \times 100$	
Conv2D	$128 \times 2 \times 26$	(1, 25)/(1, 3)	CConv2D	$2 \times 64 \times 1 \times 26$	(1, 25)/(1, 3)
BatchNorm	$128 \times 2 \times 26$		CBatchNorm	$2 \times 64 \times 1 \times 26$	
ReLU	$128 \times 2 \times 26$		CReLU	$2 \times 64 \times 1 \times 26$	
Conv2D	$20 \times 2 \times 3$	(1, 20)/(1, 3)	CConv2D	$2 \times 20 \times 1 \times 3$	(1, 20)/(1, 3)
BatchNorm	$20 \times 2 \times 3$		CBatchNorm	$2 \times 20 \times 1 \times 3$	
ReLU	$20 \times 2 \times 3$		CReLU	$2 \times 20 \times 1 \times 3$	
AvgPool2D	20	(2, 3)/(1, 1)	CAvgPool2D	$2 \times 20$	(1, 3)/(1, 1)
Cross Entropy of $x$			Cross Entropy of $ z $		

TABLE I

Details of the RVNN and CVNN architectures

We can rewrite the above equation to matrix form as:

$$\begin{bmatrix} \text{Re}(\mathbf{W} * \mathbf{h}) \\ \text{Im}(\mathbf{W} * \mathbf{h}) \end{bmatrix} = \begin{bmatrix} \mathbf{A} & -\mathbf{B} \\ \mathbf{B} & \mathbf{A} \end{bmatrix} * \begin{bmatrix} \mathbf{x} \\ \mathbf{y} \end{bmatrix} \quad (2)$$

Equation (1) shows that the complex-valued convolutional layer needs two real-valued convolutional filters  $A$  and  $B$ . For the complex-valued vector  $h$  with real part  $x$  and imaginary part  $y$ , both the real and imaginary part of the output of complex-valued convolution operator consist of these four components  $(A, B, x, y)$ . The only difference between the two is that the real part of the output is the subtraction between  $\mathbf{A} * \mathbf{x}$  and  $\mathbf{B} * \mathbf{y}$ , and the imaginary part is the addition between the cross terms  $\mathbf{B} * \mathbf{x}$  and  $\mathbf{A} * \mathbf{y}$ . This interleaving between the real and imaginary components is the most significant difference between CVNNs and RVNNs.

### C. Neural Network Architectures

Figure 2 shows the architecture of the RVNN (top) and CVNN (bottom) used in our experiments. To simplify the analysis, we used RVNNs and CVNNs with two convolutional layers; deeper networks would likely improve performance but at the cost of making the analysis much more complex. Our baseline RVNN has two real-valued convolutional layers (conv layers), with each conv layer followed by a batch normalization layer and a ReLU layer. The output of the second conv layer goes to an average pooling layer, which produces the output. We use a cross entropy loss function to train the network.

Conceptually, the CVNN has an analogous structure as the RVNN, except each layer now consists of a real-valued part and a complex-valued part. The details of both architectures can be found in Table I.

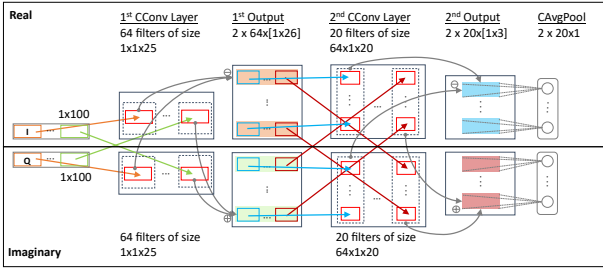
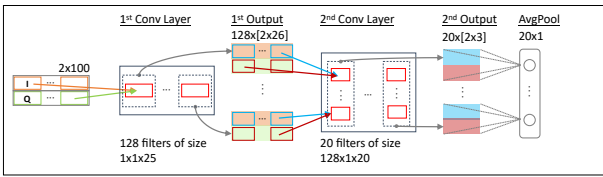


Fig. 3: The computational flow schematic for a RVNN (top) and a CVNN (bottom).

To perform a head-to-head comparison between a RVNN and an “equivalent” CVNN, we keep the number of parameters for both types of neural networks equal to each other. For instance, with the *Wired* datasets, both the RVNN and the CVNN have 54400 parameters total. However, having an equal number of parameters is not an exact “apples-to-apples” comparison as there are other architectural differences. As such, we also include experiments that change the input features and ablation experiments to shed light on the capabilities of CVNNs over RVNNs.

#### D. Ablation Strategies

The main difference between the CVNN and the RVNN is due to the cross terms between the real and imaginary parts in the multiplication and convolution operations. Figure 3 illustrates the computational flow for a RVNN (top) and a CVNN (bottom); the computational flow of a CVNN is much more complex than that of a RVNN. As a concrete example, take the first complex-valued convolutional layer (1<sup>st</sup> CConv Layer) and its associated Output (1<sup>st</sup> Output) in Figure 3b. The real part of the 1<sup>st</sup> Output (orange blocks) comes from the linear combination of I data scanned by real filters and Q data scanned by imaginary filters (as shown by the grey arrows pointing to the  $\ominus$ ), while the imaginary part of the 1<sup>st</sup> Output (green blocks) comes from the cross terms formed by the linear combination of I data scanned by imaginary filters and Q data scanned by real filters (as shown by the gray arrows pointing to  $\oplus$ ). Here the  $\ominus$  and  $\oplus$  symbols in Figure 3b correspond to the real ( $\mathbf{A} * \mathbf{x} - \mathbf{B} * \mathbf{y}$ ) and imaginary parts ( $\mathbf{B} * \mathbf{x} + \mathbf{A} * \mathbf{y}$ ) of Equation 1.

We perform a deeper analysis into the differences between the two models through a series of ablation experiments which remove parts of the CVNN, specifically parts that correspond to some of the cross terms. By “remove” we mean that we zero out the ablated component. If performance degrades significantly, then the portion of the CVNN that is removed is an important component of the model. Figure 3b

	Ablate Outputs		Ablate Conv Filters	
	Remove Re Output	Remove Im Output	Remove Re Conv	Remove Im Conv
L1 (Ablate 1 <sup>st</sup> Layer)	L1_O_RE	<b>L1_O_IM</b>	L1_C_RE	<b>L1_C_IM</b>
L2 (Ablate 2 <sup>nd</sup> Layer)	L2_O_RE	<b>L2_O_IM</b>	L2_C_RE	<b>L2_C_IM</b>
L12 (Ablate Both)	L12_O_RE	<b>L12_O_IM</b>	L12_C_RE	<b>L12_C_IM</b>

TABLE II  
Ablation Models

illustrates the CVNN as 2 layers, with each layer consisting of convolutional filters and an output. There is a set of 12 ablation experiments that can be defined by the following dimensions and values: 1) the layer to ablate: 1<sup>st</sup> layer (**L1**), 2<sup>nd</sup> layer (**L2**), or both (**L12**); 2) the component of the layer to ablate: the convolutional filter (**C**) or the output (**O**); 3) the part of the component to remove: the real part (**RE**) or the imaginary part (**IM**).

Table II summarizes the 12 ablation experiments, with the name of the experiment stated in each table cell. The naming convention follows the boldface labels chosen for each ablation dimension, concatenated with an underscore. For example, “L1\_O\_IM” ablates the 1<sup>st</sup> Output and remove the imaginary part of the output (green blocks of the 1<sup>st</sup> Output in Figure 3b). In our results, we only show results of the “IM” ablations which remove the imaginary part (of the output or convolutional filter) and keep the real part; the results of the “RE” ablations have equivalent performance.

#### E. Varying the Inputs to the Neural Networks

We also explore changing the set of inputs to the neural networks. For IQ samples, we investigate the following three configurations: 1) use only the input **I**; 2) use only the input **Q**; 3) use both I and Q (**IQ** for short) as the input. For the polar representation of IQ samples, we denote the magnitude part as **R** and the phase part as **T**. As before, we explore three configurations: 1) use only the input **R**; 2) use only the input **T**; 3) use both R and T (**RT** for short). For configurations that only provide one input, we zero out the other input.

### V. PERFORMANCE RESULTS AND ANALYSIS

In this section, we report the classification results and present the findings on the comparison between RVNN and CVNN and between the various ablation models of CVNN, using the datasets described in Section III. In addition, we investigate how the different input modes affect the performance. We present the average accuracy of each model for each dataset scenario as a bar chart, error bars ( $\pm\sigma$ ) are also shown.

#### A. RVNNs versus CVNNs

**Using IQ Data as Input:** Figure 4 shows the average classification accuracy achieved using RVNNs and CVNNs with raw IQ samples as input under each of the four dataset scenarios (LoRa/In, LoRa/Out, *Wired*, *WiFi*); CVNNs outperform RVNNs by a substantial amount (16%-34%) for all four scenarios. In the OSU-LoRa case, the LoRa/In has better performance than LoRa/Out, which is expected since Indoor signals have lesser interference compared with the Outdoor ones. For the NE-*Wired*/*WiFi* case, interestingly, our experimental results reveal that *WiFi* (Anechoic Cham-

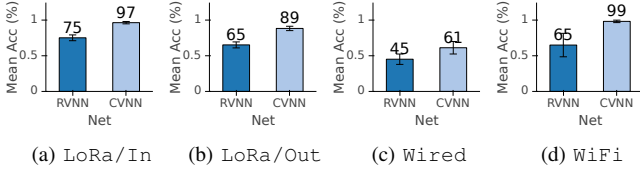


Fig. 4: RVNN vs. CVNN (Input: IQ)

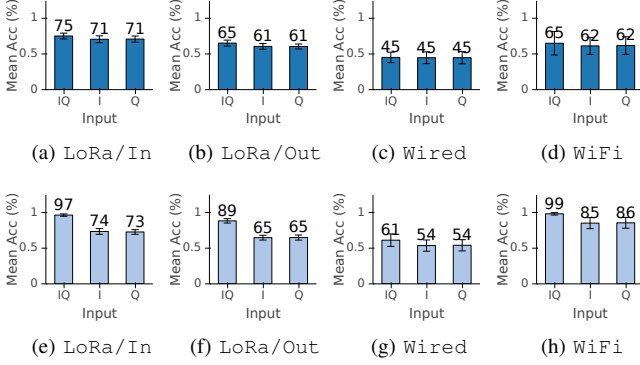


Fig. 5: IQ vs. I vs. Q. (Top: RVNN, Bottom: CVNN)

ber WiFi) achieves higher accuracy than that achieved under Wired (Wired) for both RVNN and CVNN.

**Using I vs Q vs IQ Data as Input:** Figure 5 shows the average accuracy for the RVNN (top) and CVNN (bottom) models, when considering I only, Q only, and both IQ as data input to the learning models. The figures show that the I and Q components when fed by themselves as an input to the learning model yield roughly the same average accuracy, and this is true for each of four studied datasets and each of the two models (RVNN or CVNN). This result indicates that in isolation, I and Q contain a similar amount of predictive information. Note that using both IQ as input results in a (sometimes slightly) higher accuracy, which is expected since the full input should contain more information. However, the increase in accuracy from using both IQ over using I or Q in isolation is much higher for CVNNs (7%-24%) than RVNNs (<5%). This result shows that a CVNN is able to use the joint information between I and Q more effectively than a RVNN due to the cross terms generated by the complex number multiplication and convolution operations.

**Using RT vs IQ Data as Input:** Figure 6 (top) shows that the IQ representation of the input data produces a large improvement over RT (approximately 40%) for the OSU-LoRa datasets under RVNNs. The opposite is true for the NE-Wired/WiFi datasets as the RT representation produces improvements of 28%-31% over the IQ representation. Figure 6 (bottom) shows that for CVNNs, the IQ representation produces improvements over the RT representation (4%-22%) in three datasets, with the exception being for Wired, which resulted in the IQ representation being 22% lower. When comparing RT results of CVNNs to those of RVNNs

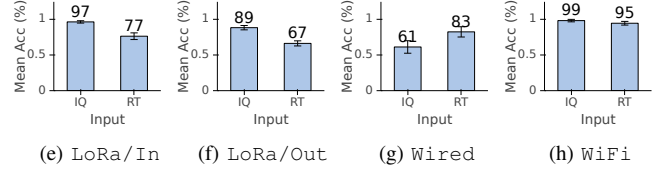
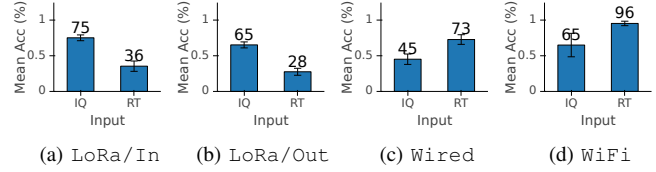


Fig. 6: IQ vs. RT. (Top: RVNN, Bottom: CVNN)

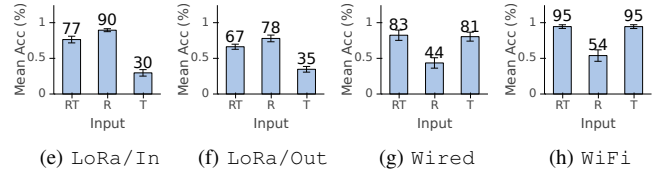
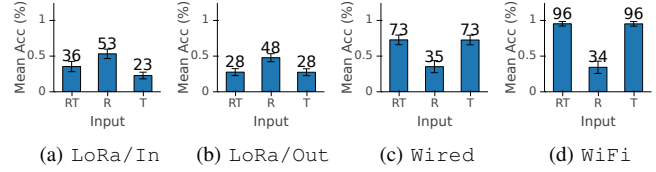


Fig. 7: RT vs. R vs. T (Top: RVNN, Bottom: CVNN)

on specific datasets, we can see that CVNNs produce an accuracy that is much higher (10%-41%) than that produced under RVNNs in all datasets except for WiFi, which yields close to equivalent accuracy.

Figure 7 shows that for OSU-LoRa datasets, having R as the only input produces large improvements in accuracy of 20%-60% compared to having only T as input and improvements of 11%-20% over having both RT as inputs. For NE-Wired/WiFi datasets, the results are the opposite. Having T as the only input produces improvements in accuracy of 37%-62% than having only R. However, having both RT as inputs is almost equivalent to the accuracy of only including T. In general, CVNNs tend to outperform the corresponding R, T or RT results on RVNNs with the exception of the RT and T results for the WiFi dataset.

### B. Ablation Analysis

Figure 8 shows the effect on accuracy from ablating components of a CVNN (in the order of L1, L2, L12) with IQ as inputs. The first row (Figures 8a-8d) shows the results of ablating the imaginary outputs and the second row (8e-8h) shows the results of ablating the imaginary convolutional filters. Figure 9 illustrates the results of the analogous experiments with RT as input.

In general, ablating the outputs produces a decreasing trend in performance (moving from L1 to L2 to L12) as shown

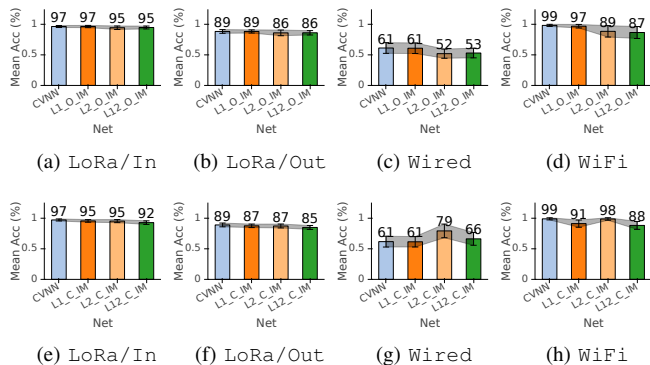


Fig. 8: Ablation analysis (Input: IQ). The top row ablates the outputs while the bottom row ablates the conv layers

in Figures 8 and 9. In multi-layer neural networks, deeper layers are known to represent higher-level features (e.g. parts and objects) rather than low-level features (e.g. texture and colors) [23]. Our results indicate that removing the 2nd layer (in experiment L2) removes a higher-level feature that is more predictive of the class label, thus resulting in a lower accuracy. In addition, by comparing the results from Figures 6, 8 and 9, we can observe that even an impoverished CVNN can produce significant gains over a RVNN.

On the other hand, ablating the convolutional filters produces a different behavior from ablating the outputs. Figures 8g (bottom) and 9f (bottom) show that the results are mixed. In some cases, removing the second layer’s imaginary filters produce the highest accuracy (e.g. Figure 8g) while in other cases, removing the first layer’s imaginary filters produce the highest accuracy (e.g. Figure 9f). We speculate that the additional cross-terms in CVNNs produce redundant information that can cause overfitting in some cases; our ablations removed this redundancy which in turn improved accuracy. In many cases, removing the convolutional layers produces a great range of differences in accuracy than removing the output layers; this difference indicates that the convolutional layers play a more important role in terms of predictive accuracy than the outputs for CVNNs.

## VI. CONCLUSION

CVNNs are a more accurate model for wireless device classification than RVNNs, with CVNNs consistently outperforming RVNNs with approximately the same number of parameters. The main benefit that CVNNs provide over RVNNs is a more effective use of the joint information between in-phase and quadrature components of the signals, with this joint information being captured by cross-terms produced by complex number operations. Finally, we also showed through ablation experiments that deeper layers of CVNNs capture important higher-level features that can improve accuracy.

## REFERENCES

[1] N. Soltanieh *et al.*, “A review of radio frequency fingerprinting techniques,” *IEEE Journal of Radio Frequency Identification*, vol. 4, pp. 222–233, 2020.

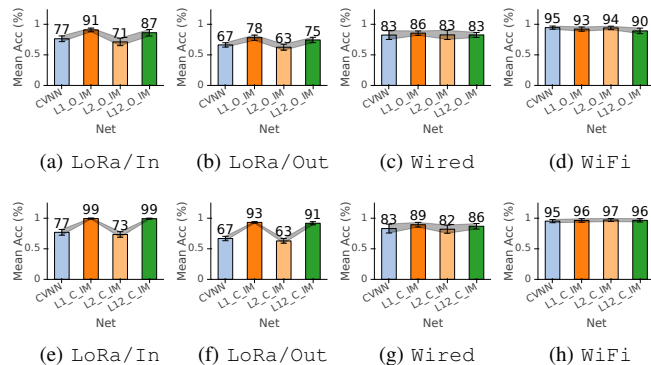


Fig. 9: Ablation analysis (Input: RT). The top row ablates the outputs while the bottom row ablates the conv layers

[2] S. Riyaz *et al.*, “Deep learning convolutional neural networks for radio identification,” *IEEE Comm. Magazine*, vol. 56, pp. 146–152, 2018.

[3] F. Restuccia *et al.*, “Deepradioid: Real-time channel-resilient optimization of deep learning-based radio fingerprinting algorithms,” *Proceedings of the Twentieth ACM International Symposium on Mobile Ad Hoc Networking and Computing*, 2019.

[4] B. Hamdaoui, A. Elmaghub, and S. Mejri, “Deep neural network feature designs for RF data-driven wireless device classification,” *IEEE Network*, vol. 35, no. 3, pp. 191–197, 2020.

[5] A. Elmaghub, B. Hamdaoui, and A. Natarajan, “Widescan: Exploiting out-of-band distortion for device classification using deep learning,” in *GLOBECOM 2020-2020 IEEE Global Communications Conference*. IEEE, 2020, pp. 1–6.

[6] T. O’Shea, J. Corgan, and T. Clancy, “Convolutional radio modulation recognition networks,” *ArXiv*, vol. abs/1602.04105, 2016.

[7] S. Gopalakrishnan, M. Cekic, and U. Madhoo, “Robust wireless fingerprinting via complex-valued neural networks,” *2019 IEEE Global Communications Conference (GLOBECOM)*, pp. 1–6, 2019.

[8] I. Agadako *et al.*, “Deep complex networks for protocol-agnostic radio frequency device fingerprinting in the wild,” *ArXiv*, vol. abs/1909.08703, 2019.

[9] N. E. West and T. O’Shea, “Deep architectures for modulation recognition,” *2017 IEEE International Symposium on Dynamic Spectrum Access Networks (DySPAN)*, pp. 1–6, 2017.

[10] T. O’Shea and J. Hoydis, “An introduction to deep learning for the physical layer,” *IEEE Transactions on Cognitive Communications and Networking*, vol. 3, pp. 563–575, 2017.

[11] J. Bao, B. Hamdaoui, and W.-K. Wong, “Iot device type identification using hybrid deep learning approach for increased iot security,” in *2020 International Wireless Communications and Mobile Computing (IWCMC)*. IEEE, 2020, pp. 565–570.

[12] K. Sankhe *et al.*, “Oracle: Optimized radio classification through convolutional neural networks,” *IEEE INFOCOM 2019 - IEEE Conference on Computer Communications*, pp. 370–378, 2019.

[13] N. Soltani *et al.*, “More is better: Data augmentation for channel-resilient rf fingerprinting,” *IEEE Communications Magazine*, vol. 58, pp. 66–72, 2020.

[14] N. Basha and B. Hamdaoui, “Leveraging multiple transmissions and receptions for channel-agnostic deep learning-based network device classification,” *arXiv preprint arXiv:2109.03799*, 2021.

[15] A. Al-Shawabka *et al.*, “Exposing the fingerprint: Dissecting the impact of the wireless channel on radio fingerprinting,” *IEEE INFOCOM 2020 - IEEE Conference on Computer Communications*, pp. 646–655, 2020.

[16] I. Agadako *et al.*, “Chameleons’ oblivion: Complex-valued deep neural networks for protocol-agnostic rf device fingerprinting,” *2020 IEEE European Symposium on Security and Privacy (EuroS&P)*, pp. 322–338, 2020.

[17] A. Elmaghub and B. Hamdaoui, “LoRa device fingerprinting in the wild: Disclosing RF data-driven fingerprint sensitivity to deployment variability,” *IEEE Access*, vol. 9, pp. 142 893–142 909, 2021.

[18] T. Nitta, “An extension of the back-propagation algorithm to complex

- numbers," *Neural networks : the official journal of the International Neural Network Society*, vol. 10 8, pp. 1391–1415, 1997.
- [19] G. Georgiou and C. Koutsougeras, "Complex domain backpropagation," *IEEE Transactions on Circuits and Systems II: Analog and Digital Signal Processing*, vol. 39, no. 5, pp. 330–334, 1992.
  - [20] H. Leung and S. Haykin, "The complex backpropagation algorithm," *IEEE Trans. Signal Process.*, vol. 39, pp. 2101–2104, 1991.
  - [21] N. Benvenuto and F. Piazza, "On the complex backpropagation algorithm," *IEEE Trans. Signal Process.*, vol. 40, pp. 967–969, 1992.
  - [22] C. Trabelsi *et al.*, "Deep complex networks," *ArXiv*, vol. abs/1705.09792, 2018.
  - [23] D. Bau *et al.*, "Network dissection: Quantifying interpretability of deep visual representations," in *CVPR*, 2017, pp. 3319–3327.